

## Spin asymmetries $A_1$ of the proton and the deuteron in the low $x$ and low $Q^2$ region from polarized high energy muon scattering

B. Adeva,<sup>18</sup> E. Arik,<sup>2</sup> A. Arvidson,<sup>21,a</sup> B. Badełek,<sup>21,23</sup> G. Baum,<sup>1</sup> P. Berglund,<sup>8</sup> L. Betev,<sup>13,b</sup> R. Birsa,<sup>20</sup> N. de Botton,<sup>17</sup> F. Bradamante,<sup>20</sup> A. Bravar,<sup>11</sup> S. Bültmann,<sup>1,c</sup> E. Burtin,<sup>17</sup> D. Crabb,<sup>22</sup> J. Cranshaw,<sup>20,f</sup> T. Çuhadar,<sup>2,15</sup> S. Dalla Torre,<sup>20</sup> R. van Dantzig,<sup>15</sup> B. Derro,<sup>4</sup> A. Deshpande,<sup>24</sup> S. Dhawan,<sup>24</sup> C. Dulya,<sup>4,e</sup> S. Eichblatt,<sup>f</sup> D. Fasching,<sup>16,g</sup> F. Feinstein,<sup>17</sup> C. Fernandez,<sup>20,9</sup> B. Froise,<sup>17</sup> A. Gallas,<sup>20</sup> J. A. Garzon,<sup>20,9</sup> H. Gilly,<sup>6</sup> M. Giorgi,<sup>22</sup> S. Goertz,<sup>3</sup> G. Garcia,<sup>20,h</sup> N. de Groot,<sup>15,i</sup> M. Grosse Perdekamp,<sup>24,j</sup> K. Haft,<sup>13</sup> D. von Harrach,<sup>11</sup> T. Hasegawa,<sup>14,k</sup> P. Hautle,<sup>5,l</sup> N. Hayashi,<sup>14,m</sup> C. A. Heusch,<sup>5,n</sup> N. Horikawa,<sup>14</sup> V. W. Hughes,<sup>24</sup> G. Igo,<sup>4</sup> S. Ishimoto,<sup>14,o</sup> T. Iwata,<sup>14</sup> E. M. Kabuß,<sup>11</sup> A. Karev,<sup>10</sup> H. J. Kessler,<sup>6,p</sup> T. J. Ketel,<sup>15</sup> J. Kiryluk,<sup>21,23</sup> Yu. Kisselev,<sup>10</sup> D. Krämer,<sup>1</sup> W. Kröger,<sup>5,n</sup> K. Kurek,<sup>23</sup> J. Kynäräinen,<sup>1,8</sup> M. Lamanna,<sup>20,q</sup> U. Landgraf,<sup>6</sup> J. M. Le Goff,<sup>17</sup> F. Lehar,<sup>17</sup> A. de Lesquen,<sup>17</sup> J. Lichtenstadt,<sup>19</sup> M. Litmaath,<sup>15,q</sup> A. Magnon,<sup>19</sup> G. K. Mallot,<sup>11,q</sup> F. Marie,<sup>17</sup> A. Martin,<sup>20</sup> J. Martino,<sup>17</sup> T. Matsuda,<sup>14,k</sup> B. Mayes,<sup>9</sup> J. S. McCarthy,<sup>22</sup> K. Medved,<sup>10</sup> W. Meyer,<sup>3</sup> G. van Middelkoop,<sup>15</sup> D. Miller,<sup>16</sup> Y. Miyachi,<sup>14</sup> K. Mori,<sup>14</sup> J. Nassalski,<sup>23</sup> T. O. Niinikoski,<sup>5</sup> J. E. J. Oberski,<sup>15</sup> A. Ogawa,<sup>14,r</sup> C. Ozben,<sup>2</sup> H. Pereira,<sup>17</sup> F. Perrot-Kunne,<sup>17</sup> D. Peshekhonov,<sup>10,d</sup> R. Piegaia,<sup>24,s</sup> L. Pinsky,<sup>9</sup> S. Platchkov,<sup>17</sup> M. Plo,<sup>18</sup> D. Pose,<sup>10</sup> H. Postma,<sup>15</sup> J. Pretz,<sup>11,t</sup> R. Puntaferro,<sup>20</sup> G. Rädcl,<sup>5,u</sup> G. Reicherz,<sup>3</sup> J. Roberts,<sup>v</sup> M. Rodriguez,<sup>21,s</sup> E. Rondio,<sup>23</sup> I. Sabo,<sup>19</sup> J. Saborido,<sup>18</sup> A. Sandacz,<sup>23</sup> I. Savin,<sup>10</sup> P. Schiavon,<sup>20</sup> E. P. Sichtermann,<sup>15</sup> F. Simeoni,<sup>20</sup> G. I. Smirnov,<sup>10</sup> A. Staude,<sup>13</sup> A. Steinmetz,<sup>11,t</sup> U. Stiegler,<sup>5</sup> H. Stuhmann,<sup>7</sup> F. Tessarotto,<sup>20</sup> D. Thers,<sup>17</sup> W. Tłaczala,<sup>23,w</sup> A. Tripet,<sup>1</sup> G. Unel,<sup>2</sup> M. Velasco,<sup>15,q</sup> J. Vogt,<sup>13</sup> R. Voss,<sup>5</sup> C. Whitten,<sup>4</sup> R. Willumeit,<sup>7</sup> R. Windmolders,<sup>12</sup> W. Wiślicki,<sup>23</sup> A. Witzmann,<sup>6,x</sup> A. M. Zanetti,<sup>20</sup> K. Zaremba,<sup>23,w</sup> and J. Zhao<sup>7,y</sup>

(Spin Muon Collaboration)

<sup>1</sup>University of Bielefeld, Physics Department, D-33501 Bielefeld, Germany

<sup>2</sup>Bogaziçi University and Istanbul Technical University, 80676 Istanbul, Turkey

<sup>3</sup>University of Bochum, Physics Department, D-44780 Bochum, Germany

<sup>4</sup>University of California, Department of Physics, Los Angeles, California 90024

<sup>5</sup>CERN, CH-1211 Geneva 23, Switzerland

<sup>6</sup>University of Freiburg, Physics Department, D-79104 Freiburg, Germany

<sup>7</sup>GKSS, D-21494 Geesthacht, Germany

<sup>8</sup>Helsinki University of Technology, Low Temperature Laboratory and Institute of Particle Physics Technology, 02150 Espoo, Finland

<sup>9</sup>University of Houston, Department of Physics and Institute for Beam Particle Dynamics, Houston, Texas 77204

<sup>10</sup>JINR, Dubna, RU-141980 Dubna, Russia

<sup>11</sup>University of Mainz, Institute for Nuclear Physics, D-55099 Mainz, Germany

<sup>12</sup>University of Mons, Faculty of Science, B-7000 Mons, Belgium

<sup>13</sup>University of Munich, Physics Department, D-80799 Munich, Germany

<sup>14</sup>Nagoya University, CIRSE and Department of Physics, Furo-Cho, Chikusa-Ku, 464 Nagoya, Japan

<sup>15</sup>NIKHEF, Delft University of Technology, FOM and Free University, 1009 AJ Amsterdam, The Netherlands

<sup>16</sup>Northwestern University, Department of Physics, Evanston, Illinois 60208

<sup>17</sup>C.E.A. Saclay, DAPNIA, F-91191 Gif-sur-Yvette, France

<sup>18</sup>University of Santiago, Department of Particle Physics, E-15706 Santiago de Compostela, Spain

<sup>19</sup>Tel Aviv University, School of Physics, 69978 Tel Aviv, Israel

<sup>20</sup>INFN Trieste and University of Trieste, Department of Physics, I-34127 Trieste, Italy

<sup>21</sup>Uppsala University, Department of Radiation Sciences, S-75121 Uppsala, Sweden

<sup>22</sup>University of Virginia, Department of Physics, Charlottesville, Virginia 22901

<sup>23</sup>Soltan Institute for Nuclear Studies and Warsaw University, PL-00681 Warsaw, Poland

<sup>24</sup>Yale University, Department of Physics, New Haven, Connecticut 06520

(Received 22 April 1999; published 13 September 1999)

We present the results of the spin asymmetries  $A_1$  of the proton and the deuteron in the kinematic region extending down to  $x = 6 \times 10^{-5}$  and  $Q^2 = 0.01 \text{ GeV}^2$ . The data were taken with a dedicated low  $x$  trigger, which required hadron detection in addition to the scattered muon, so as to reduce the background at low  $x$ . The results complement our previous measurements and the two sets are consistent in the overlap region. No significant spin effects are found in the newly explored region. [S0556-2821(99)02617-X]

PACS number(s): 13.60.Hb, 13.88.+e

## I. INTRODUCTION

Polarized deep inelastic lepton-nucleon scattering is an important tool to study the spin structure of the nucleon. Measurements with polarized proton, deuteron, and helium-3 targets have determined the spin-dependent structure functions of the nucleon in a wide kinematic range. In this paper we present results for the virtual photon-proton and virtual photon-deuteron cross section asymmetries  $A_1^p$  and  $A_1^d$  obtained from inelastic muon-proton and muon-deuteron inter-

<sup>a</sup>Present address: The Royal Library, S-102 41 Stockholm, Sweden.

<sup>b</sup>Present address: University of California, Department of Physics, Los Angeles, CA 90024; USA permanent address: CERN, C4-1211 Geneva 23, Switzerland.

<sup>c</sup>Present address: University of Virginia, Department of Physics, Charlottesville, VA 22901.

<sup>d</sup>Present address: Texas Technical University, Lubbock, TX 79409-1051.

<sup>e</sup>Present address: CIEMAT, Avda Complutense 22, E-28040, Madrid, Spain.

<sup>f</sup>Present address: Fermi National Accelerator Laboratory, Batavia, IL 60510.

<sup>g</sup>Present address: University of Wisconsin, Madison, WI 53706.

<sup>h</sup>Present address: NIKHEF, 1009 AJ Amsterdam, The Netherlands.

<sup>i</sup>Present address: Bristol University, Bristol, BS8 1TL United Kingdom.

<sup>j</sup>Present address: Brookhaven National Laboratory, Upton, NY 11973.

<sup>k</sup>Permanent address: Miyazaki University, Faculty of Engineering, 889-21 Miyazaki-Shi, Japan.

<sup>l</sup>Permanent address: Paul Scherrer Institut, CH-5232 Villigen, Switzerland.

<sup>m</sup>Permanent address: The Institute of Physical and Chemical Research (RIKEN), wako 351-01, Japan.

<sup>n</sup>Permanent address: University of California, Institute of Particle Physics, Santa Cruz, CA 95064.

<sup>o</sup>Permanent address: KEK, Tsukuba-Shi, 305 Ibaraki-Ken, Japan.

<sup>p</sup>Present address: SBC Warburg Dillon Read, CH-4002 Basel, Switzerland.

<sup>q</sup>Present address: CERN, CH-1211 Geneva 23, Switzerland.

<sup>r</sup>Present address: Pennsylvania State University, University Park, PA 16802.

<sup>s</sup>Permanent address: University of Buenos Aires, Physics Department, 1428 Buenos Aires, Argentina.

<sup>t</sup>Present address: Yale University, Department of Physics, New Haven, CT 06520.

<sup>u</sup>Present Address: CEA Saclay, DAPNIA, F91191 Gif-sur-Yvette, France.

<sup>v</sup>Permanent address: Rice University, Bonner Laboratory, Houston, TX 77251-1892.

<sup>w</sup>Permanent address: Warsaw University of Technology, PL-00-665 Warsaw, Poland.

<sup>x</sup>Present address: F. Hoffmann-La Roche Ltd., CH-4070 Basel, Switzerland.

<sup>y</sup>Present address: Oak Ridge National Laboratory, Oak Ridge, TN 37831-6393.

actions at 190 GeV, at very low  $x$  and  $Q^2$ , extending our measurements down to  $x = 6 \times 10^{-5}$ . The data were collected with a ‘‘low  $x$  trigger’’ in which both a minimal energy deposit in the hadronic part of the calorimeter and the detection of a scattered muon were demanded. The hadron requirement reduces the background at low  $x$ , which is dominated by contamination from muon scattering off atomic electrons at  $x_{\mu e} = m_e/M_p$  and by radiative events.

The physics of high parton densities, i.e., at low values of  $x$ , is being studied intensively [1]. The measurements at the DESY  $ep$  collider HERA show [2] that the rise of the spin-independent structure function  $F_2$  with decreasing  $x$  is present even at the smallest values of  $Q^2$ ,  $Q^2 \sim 0.1 \text{ GeV}^2$ . For  $Q^2 \gtrsim 1 \text{ GeV}^2$ , that rise can be described by the standard Dokshitzer-Gribov-Lipatov-Altarelli-Parisi: (DGLAP) QCD evolution. In the nonperturbative region ( $Q^2 \lesssim 1 \text{ GeV}^2$ ) several approaches have been proposed [1,3] to join leptoproduction to photoproduction ( $Q^2 = 0 \text{ GeV}^2$ ).

Our new data cover the kinematic range  $6 \times 10^{-5} < x < 0.15$  and  $0.01 < Q^2 < 20 \text{ GeV}^2$ . They provide the first values of spin asymmetries below  $x = 8 \times 10^{-4}$  and complement our recently published measurements [4] that were obtained in the region  $8 \times 10^{-4} < x < 0.7$  and  $0.2 < Q^2 < 100 \text{ GeV}^2$ .

## II. SPIN ASYMMETRIES

The virtual photon-proton (-deuteron) asymmetries  $A_1^{p,d}$  are defined as follows (see Ref. [5] for details):

$$A_1^p = \frac{\sigma_{1/2} - \sigma_{3/2}}{\sigma_{1/2} + \sigma_{3/2}}, \quad A_1^d = \frac{\frac{1}{2}(\sigma_0 - \sigma_2)}{\frac{1}{3}(\sigma_0 + \sigma_1 + \sigma_2)}, \quad (1)$$

where  $\sigma_J$  is the absorption cross section of a transverse virtual photon by a proton (deuteron) with total spin projection  $J$  in the photon direction.

In the spin muon collaboration (SMC) experiment, cross section asymmetries for parallel and antiparallel configurations of longitudinal beam and target polarizations,

$$A_{\parallel}^{p,d} = \frac{\sigma^{\uparrow\downarrow} - \sigma^{\uparrow\uparrow}}{\sigma^{\uparrow\downarrow} + \sigma^{\uparrow\uparrow}}, \quad (2)$$

are determined. They are related to the spin asymmetries  $A_1^{p,d}$  and  $A_2^{p,d}$  in the following way [5]:

$$A_{\parallel}^{p,d} = D(A_1^{p,d} + \eta A_2^{p,d}), \quad (3)$$

where  $D$  is the depolarization factor and  $\eta$  depends only on kinematic variables. In the kinematic region of our measurements,  $\eta$  is small. This together with small values of the asymmetries  $A_2^{p,d}$  published in Ref. [6] allows us to neglect the second term in Eq. (3) and to account for it only in the systematic error estimate.

The definition of the depolarization factor  $D$  requires care. The present measurements extend to  $Q^2$  values close to the kinematic limit  $Q_{\min}^2 \approx m_{\mu}^2 y^2 / (1-y)$ , where the scattering angle is zero [ $y = (E - E')/E = \nu/E$ ]. In this case one cannot neglect terms proportional to the muon mass squared in the expression for the cross section. One should also observe that in the relation (3) between  $A_{\parallel}$ ,  $D$ , and  $A_{1,2}$ , only  $A_{\parallel}$  is an observable, directly connected to the cross section. Therefore the muon mass term can be included in the definition of-

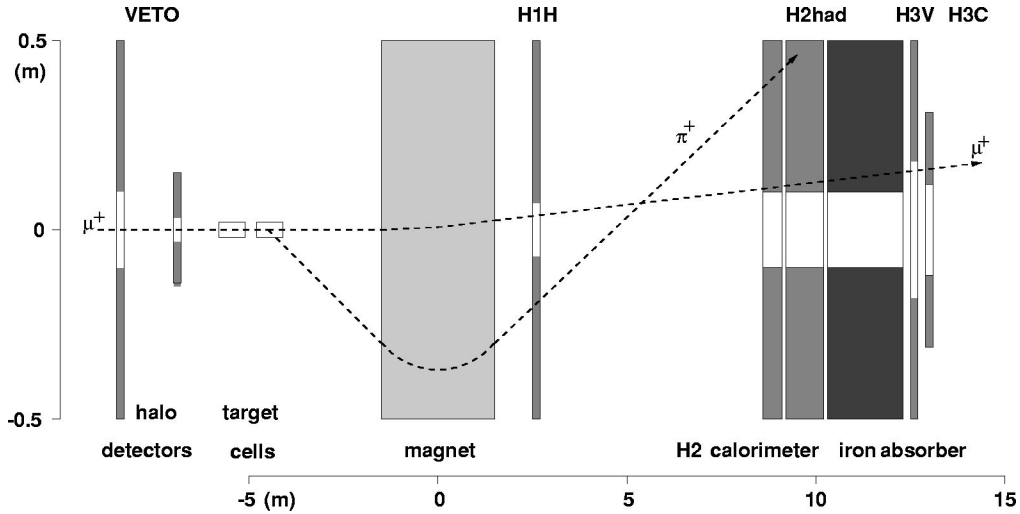


FIG. 1. The detectors used for the definition of the low  $x$  trigger: the view is in the bending plane of the magnet. The detector planes and the beam holes within  $\pm 0.5$  m from the  $\mu^+$ -beam axis are indicated. The vertical scale is expanded by factor of 10 with respect to the horizontal one.

either  $D$  or  $A_{1,2}$ , provided their product,  $A_{\parallel}$ , remains unchanged. We have chosen the former option in order to keep the definition of  $A_1$  consistent with the one used in our previous publications, so that the depolarization factor  $D$  is defined as in Ref. [5]:

$$D = \frac{y(2-y)(1+\gamma^2 y/2)}{y^2(1+\gamma^2)(1-2m_\mu^2/Q^2)+2(1-y-\gamma^2 y^2/4)(1+R)}, \quad (4)$$

where  $\gamma = \sqrt{Q^2}/\nu$  and  $R = \sigma_L/\sigma_T$  is the ratio of the absorption cross sections for longitudinal and transverse virtual photons. With this definition,  $D$  becomes larger than unity at  $Q^2$  close to  $Q_{\min}^2$  and can no longer be interpreted as the fraction of the incident muon polarization carried by the virtual photon.

### III. EXPERIMENTAL SETUP

The experiment was performed at the high energy muon beam [7] at CERN. The setup consisted of (i) a large cryogenic target [8] with two cells containing target material polarized in opposite directions, (ii) an open magnetic spectrometer [5] for the measurement of scattered muons and produced hadrons, and (iii) a beam polarimeter [9]. The beam polarization was  $P_\mu = -0.795 \pm 0.019$  for an average muon energy of 187.4 GeV. For the polarized proton and deuteron targets, the materials used were ammonia ( $\text{NH}_3$ ) and deuterated butanol ( $\text{C}_4\text{D}_9\text{OD}$ ), respectively. The average proton and deuteron polarizations were 0.89 and 0.50 and were measured with relative accuracies of 2.7% and 2.1%, respectively. Events originating from both target cells were recorded simultaneously, and the target spin orientations were reversed every 5 h.

A dedicated low  $x$  trigger was used during data taking in 1995 and 1996. In addition to a scattered muon it required a hadron detected in the large calorimeter H2 [10], situated downstream of the spectrometer magnet (see Fig. 1). The

low  $x$  trigger,

$$\text{trigger} = \text{H1H} \times \text{H2had} \times (\text{H3V} \cup \text{H3C}) \times \overline{\Sigma\text{VETO}}, \quad (5)$$

was defined by the coincidence of signals from the scintillator hodoscope H1H, the hadronic part of the calorimeter H2had, the scintillator hodoscopes H3V or H3C, and the anticoincidence with  $\Sigma\text{VETO}$ . The coincidence H1H  $\times$  H2had selected the charged hadrons, a hit in either one of H3V or H3C selected scattered muons and the anticoincidence with  $\Sigma\text{VETO}$  prevented signals from halo muons already detected upstream of the target. The calorimeter H2, extending from 8.7 to 10.2 m from the magnet, had a beam hole of 20 cm diameter, while the hodoscope H3C was located at 13 m from the magnet and had a beam hole of 23 cm.

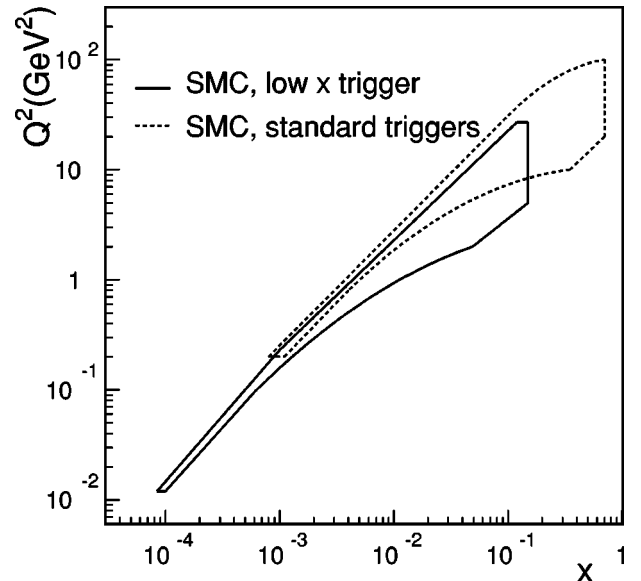


FIG. 2. Contours of the kinematic acceptance in the  $(x, Q^2)$  plane for the standard triggers (dotted line) and for the low  $x$  trigger (solid line).

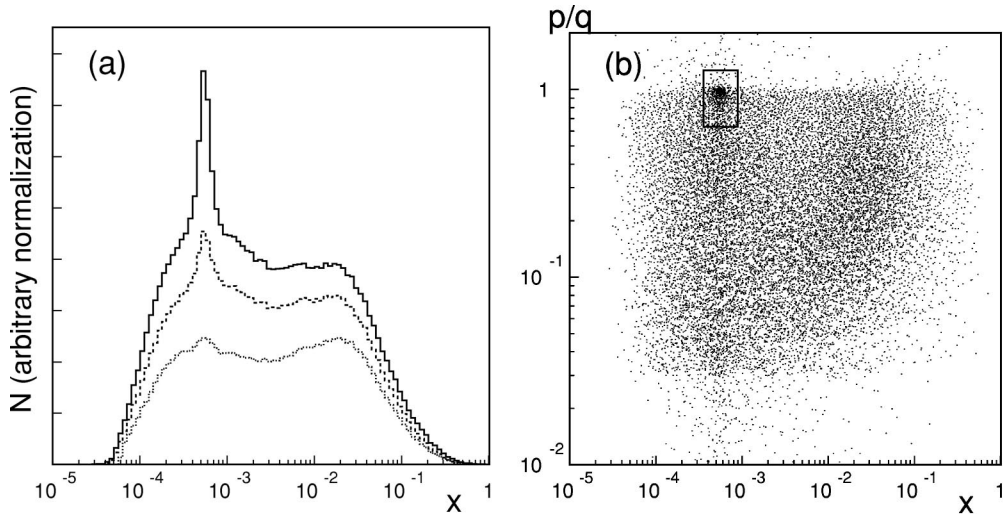


FIG. 3. (a) Event distributions as functions of  $x$  for the low  $x$  trigger without (solid histogram) and with the requirement of a reconstructed hadron (dashed histogram) and after kinematic cuts discussed in the text (dotted histogram). (b) The ratio of the particle momentum  $p$  to the momentum transfer  $q = |\vec{p}_\mu - \vec{p}'_\mu|$  vs  $x$  for the low  $x$  trigger events with only one negative particle detected. Events within the box around  $p/q = 1$  were removed from the sample.

The threshold for the calorimeter signal was on average 10 times the pulse height for muons. Nevertheless, some contamination of the trigger by events without hadrons was observed. This was presumably due to electron showers produced by the beam scraping the sides of the calorimeter or the absorber hole. The rate of the low  $x$  triggers was about 500 events per beam spill of  $4.5 \times 10^7$  muons. They were prescaled by a factor of 8 for the deuteron run and a factor of 4 for the proton run. Very small muon scattering angles, including zero, were accepted for large energy transfers,  $\nu > 110$  GeV, because the outgoing muons were deflected from the beam by the spectrometer magnet ( $\int B dl = 4.4$  Tm) and subsequently detected in H3V or H3C. This allowed the registration of events with values of  $x$  as low as  $10^{-5}$ , extending the range of the standard triggers used in our previous analyses [4]. Those standard triggers were based exclusively on the detection of scattered muons and optimized for events with  $x > 10^{-3}$  to avoid background from  $\mu e$  scattering.

The kinematic ranges in  $x$  and  $Q^2$  covered by the low  $x$  trigger data and those from the standard triggers [4] are shown in Fig. 2. For the new data most events have  $x < 0.01$ . As for all the fixed target experiments, the data at low values of  $x$  also have low values of  $Q^2$ .

**IV. EVENT SELECTION**

For the event selection, in addition to the criteria on the scattered muon (discussed later), the presence of additional particles with reconstructed tracks was required. For at least one such particle per event, a minimum of 20% of its energy was required to have been deposited in the hadronic part of the calorimeter and this deposit was demanded to be larger than 1 GeV. This eliminated most of the electrons from the sample. The tracks had to be associated with the primary interaction vertex or with a secondary vertex formed by the

decay products of neutral hadrons.

The  $x$  distributions for all events from the low  $x$  trigger and for the subsample with at least one track satisfying the above criteria are compared in Fig. 3(a). The peak at  $x_{\mu e} = m_e/M_p = 5.45 \times 10^{-4}$  corresponds to elastic scatters of muons off atomic electrons. This contamination was reduced by the event selection described above. To reduce it further an additional cut was applied to the class of events with exactly two tracks, a muon and a negatively charged particle. Figure 3(b) shows the ratio of the particle momentum  $p$  to the momentum transfer  $q = |\vec{p}_\mu - \vec{p}'_\mu|$  as a function of  $x$  for

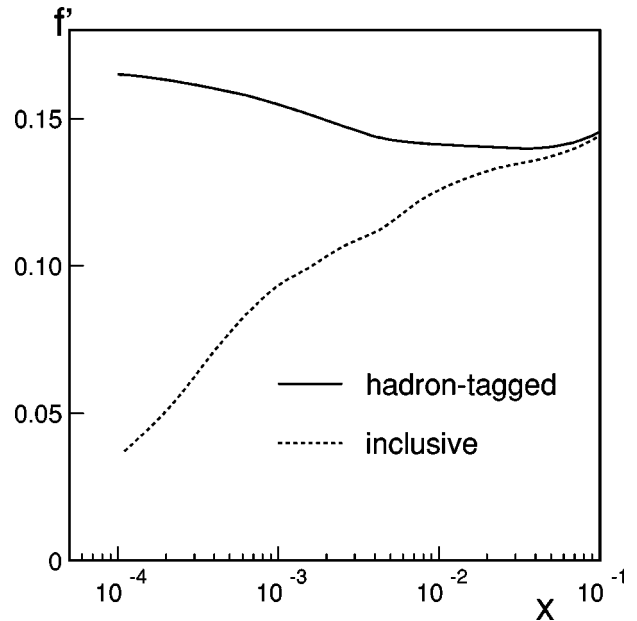


FIG. 4. The effective dilution factor  $f'(x)$  for the ammonia target for events with hadrons (solid line) and for inclusive events (dotted line).

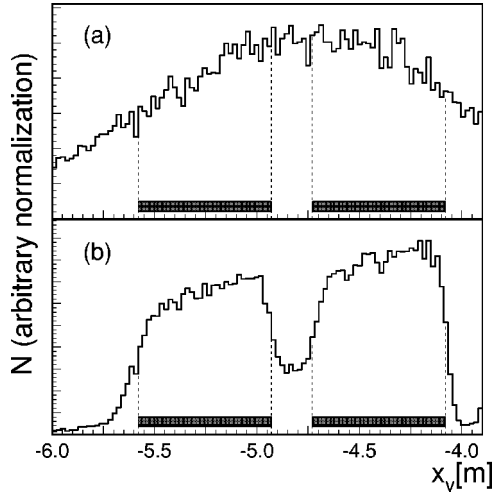


FIG. 5. Distribution of the reconstructed vertex positions along the beam direction for events after kinematic cuts, in the lowest  $x$  interval ( $6 \times 10^{-5} < x < 15 \times 10^{-5}$ ): (a) distribution of vertices reconstructed using only incoming and outgoing muon tracks and (b) distribution of vertices reconstructed using hadron tracks, too. The shaded boxes indicate the positions of the target cells. In between there is also a substantial contribution of events originating from the helium cooling liquid.

these events. Here  $\vec{p}_\mu$  and  $\vec{p}'_\mu$  denote incident and scattered muon momenta. The cluster of events around  $p/q=1$  and  $x=x_{\mu e}$  corresponds to  $\mu e$  scatters and was removed by cuts consistent with  $\mu e$  reaction kinematics:  $3.55 \times 10^{-4} < x < 8.90 \times 10^{-4}$  and  $0.63 < p/q < 1.27$ . The remaining admixture of  $\mu e$  events [cf. Fig. 3(a)], in particular those accompanied by a photon radiated by the electron, was estimated to be  $(5 \pm 1)\%$ .

The analysis is limited to the kinematic region  $x >$

$6 \times 10^{-5}$  and  $Q^2 > 0.01 \text{ GeV}^2$ . The remaining cuts, listed below, are the same as those in the analysis of Ref. [4]. The momentum of the scattered muon was restricted to  $p'_\mu > 19 \text{ GeV}$  to avoid contamination by muons from the decay of pions and kaons produced in the target. The cut on the energy transfer to the nucleon,  $\nu > 15 \text{ GeV}$ , rejects events with poor kinematic resolution, while the cut  $y = \nu/E < 0.9$  removes events which would require large radiative corrections. Cuts on the vertex position were used to select interactions from the target material. A few percent of the data were discarded because of instabilities in the beam intensity, detector efficiencies, and low target polarization. Effectively the above cuts removed about 50% of the data. The final samples of the low  $x$  trigger events consisted of  $\sim 4.5 \times 10^6$  events for polarized protons and  $\sim 1.4 \times 10^6$  events for polarized deuterons. In the newly explored range  $6 \times 10^{-5} < x < 8 \times 10^{-4}$ , this amounts to  $1.4 \times 10^6$  and  $0.5 \times 10^6$  events for the proton and the deuteron, respectively.

## V. ASYMMETRY DETERMINATION

In order to determine  $A_\parallel$  accurately, in particular when its values are small, the counting rate asymmetry  $A_\parallel^{\text{meas}}$  is evaluated by combining data sets taken before and after a reversal of the target polarization [5]. The measured asymmetry is related to the cross section asymmetry  $A_\parallel$  by  $A_\parallel^{\text{meas}} = f P_t P_\mu A_\parallel$ . The determination of  $A_\parallel$  thus requires knowledge of the incident muon and target nucleon polarizations,  $P_\mu$  and  $P_t$ , respectively, and the dilution factor  $f$  which accounts for the fact that only a fraction of the target nucleons is polarizable.

The presence of hadrons in the final state of the interaction reduces the number of events which do not carry information on the internal structure of the nucleon. There are two

TABLE I. Contributions to the systematic error on  $A_1^p(x)$  from the uncertainties in the false asymmetry  $\Delta A_{\text{false}}$ ; the target and the beam polarizations  $\Delta P_t$  and  $\Delta P_\mu$ ; the effective dilution factor  $\Delta f'$ ; the radiative corrections  $\Delta \text{rc}$ ; the neglect of  $A_2$ ,  $\Delta A_2$ ; the ratio  $R$ ,  $\Delta R$ ; and the background from polarized  $^{14}\text{N}$  in the ammonia target,  $\Delta P_{\text{bg}}$ .

| $\langle x \rangle$ | $\Delta A_{\text{false}}$ | $\Delta P_t$ | $\Delta P_\mu$ | $\Delta f'$ | $\Delta \text{rc}$ | $\Delta A_2$ | $\Delta R$ | $\Delta P_{\text{bg}}$ |
|---------------------|---------------------------|--------------|----------------|-------------|--------------------|--------------|------------|------------------------|
| 0.00010             | 0.0009                    | 0.0005       | 0.0004         | 0.0014      | 0.0008             | 0.0000       | 0.0076     | 0.0009                 |
| 0.00022             | 0.0011                    | 0.0004       | 0.0003         | 0.0011      | 0.0006             | 0.0001       | 0.0045     | 0.0009                 |
| 0.00039             | 0.0013                    | 0.0001       | 0.0000         | 0.0001      | 0.0006             | 0.0001       | 0.0005     | 0.0009                 |
| 0.00063             | 0.0014                    | 0.0001       | 0.0001         | 0.0002      | 0.0006             | 0.0002       | 0.0009     | 0.0009                 |
| 0.0010              | 0.0014                    | 0.0006       | 0.0005         | 0.0008      | 0.0007             | 0.0003       | 0.0048     | 0.0009                 |
| 0.0016              | 0.0014                    | 0.0014       | 0.0011         | 0.0014      | 0.0007             | 0.0005       | 0.0096     | 0.0008                 |
| 0.0025              | 0.0015                    | 0.0005       | 0.0004         | 0.0006      | 0.0007             | 0.0008       | 0.0036     | 0.0008                 |
| 0.0043              | 0.0018                    | 0.0002       | 0.0002         | 0.0002      | 0.0008             | 0.0008       | 0.0003     | 0.0007                 |
| 0.0078              | 0.0018                    | 0.0009       | 0.0007         | 0.0006      | 0.0008             | 0.0010       | 0.0011     | 0.0006                 |
| 0.0143              | 0.0019                    | 0.0027       | 0.0021         | 0.0018      | 0.0007             | 0.0012       | 0.0033     | 0.0006                 |
| 0.0245              | 0.0020                    | 0.0022       | 0.0017         | 0.0015      | 0.0007             | 0.0003       | 0.0043     | 0.0005                 |
| 0.0346              | 0.0020                    | 0.0032       | 0.0025         | 0.0022      | 0.0007             | 0.0003       | 0.0050     | 0.0004                 |
| 0.0487              | 0.0020                    | 0.0009       | 0.0007         | 0.0006      | 0.0008             | 0.0004       | 0.0013     | 0.0004                 |
| 0.077               | 0.0020                    | 0.0074       | 0.0058         | 0.0048      | 0.0009             | 0.0004       | 0.0114     | 0.0006                 |
| 0.121               | 0.0020                    | 0.0104       | 0.0081         | 0.0068      | 0.0010             | 0.0004       | 0.0129     | 0.0009                 |

TABLE II. Contributions to the systematic error on  $A_1^d(x)$ , with the same explanations as for Table I, except that  $\Delta P_{\text{bg}}$  now refers to the contribution from protons in the deuterated butanol target.

| $\langle x \rangle$ | $\Delta A_{\text{false}}$ | $\Delta P_t$ | $\Delta P_\mu$ | $\Delta f'$ | $\Delta \text{rc}$ | $\Delta A_2$ | $\Delta R$ | $\Delta P_{\text{bg}}$ |
|---------------------|---------------------------|--------------|----------------|-------------|--------------------|--------------|------------|------------------------|
| 0.00010             | 0.0028                    | 0.0001       | 0.0002         | 0.0007      | 0.0009             | 0.0000       | 0.0033     | 0.0002                 |
| 0.00022             | 0.0034                    | 0.0010       | 0.0011         | 0.0035      | 0.0007             | 0.0001       | 0.0146     | 0.0002                 |
| 0.00039             | 0.0038                    | 0.0005       | 0.0006         | 0.0015      | 0.0007             | 0.0001       | 0.0069     | 0.0002                 |
| 0.00063             | 0.0041                    | 0.0009       | 0.0010         | 0.0023      | 0.0007             | 0.0002       | 0.0103     | 0.0002                 |
| 0.0010              | 0.0041                    | 0.0006       | 0.0007         | 0.0011      | 0.0008             | 0.0003       | 0.0069     | 0.0002                 |
| 0.0016              | 0.0043                    | 0.0011       | 0.0013         | 0.0015      | 0.0008             | 0.0005       | 0.0113     | 0.0002                 |
| 0.0025              | 0.0045                    | 0.0002       | 0.0003         | 0.0003      | 0.0008             | 0.0008       | 0.0024     | 0.0002                 |
| 0.0043              | 0.0052                    | 0.0002       | 0.0002         | 0.0002      | 0.0009             | 0.0007       | 0.0004     | 0.0002                 |
| 0.0078              | 0.0055                    | 0.0008       | 0.0009         | 0.0008      | 0.0009             | 0.0008       | 0.0015     | 0.0002                 |
| 0.0143              | 0.0057                    | 0.0020       | 0.0023         | 0.0020      | 0.0009             | 0.0010       | 0.0035     | 0.0002                 |
| 0.0245              | 0.0060                    | 0.0002       | 0.0002         | 0.0002      | 0.0009             | 0.0015       | 0.0005     | 0.0002                 |
| 0.0346              | 0.0061                    | 0.0003       | 0.0003         | 0.0003      | 0.0009             | 0.0015       | 0.0006     | 0.0003                 |
| 0.0487              | 0.0062                    | 0.0012       | 0.0014         | 0.0012      | 0.0010             | 0.0016       | 0.0025     | 0.0004                 |
| 0.077               | 0.0063                    | 0.0014       | 0.0017         | 0.0013      | 0.0012             | 0.0004       | 0.0033     | 0.0006                 |
| 0.121               | 0.0062                    | 0.0000       | 0.0001         | 0.0000      | 0.0014             | 0.0004       | 0.0000     | 0.0008                 |

classes of such events. The first class consists of events from elastic scattering of muons off atomic electrons. The second class contains radiative events in which (quasi)elastic scattering on target nuclei is accompanied by the radiation of a hard photon. These radiative events dilute the asymmetry similarly to the interactions on nonpolarizable target nuclei. The effective dilution factor  $f'$ ,

$$f' = \frac{\sigma_{1\gamma}^{p,d}}{\sigma^{p,d}} f = \frac{n_{p,d} \sigma_{1\gamma}^{p,d}}{\sum_A n_A \sigma^A}, \quad (6)$$

accounts for these diluting sources. The sum runs over all target nuclei including protons or deuterons,  $n_{p,d,A}$  are the numbers of nuclei of a given type in the target,  $\sigma_{1\gamma}^{p,d}$  are the one-photon-exchange (Born) cross sections, and  $\sigma^{p,d,A}$  are the sums of cross sections for all processes contributing to the selected sample of events. The sum in the denominator is smaller for muon scattering with hadron production than for the inclusive muon scattering. Therefore the effective dilution factor for events with hadrons is larger than for the inclusive sample, in particular at low  $x$ , as can be seen in Fig. 4. To obtain  $f'$  the cross sections were taken from the measurements of the structure function ratios of Refs. [11,12] and the calculations of Refs. [13,14]. In addition, for the bin  $5 \times 10^{-4} < x < 8 \times 10^{-4}$ , the effective dilution factor is reduced by 5% to account for the admixture of the  $\mu$ - $e$  elastic scatterings.

The finite resolution in the vertex position affects the separation of events originating from oppositely polarized target cells and results in more dilution. The vertex resolution depends on the scattering angle, thus on  $x$ , and is improved by the use of additional tracks for the vertex determination. The improvement is particularly important at low  $x$ . If only muon tracks were used to determine the vertex position for very small scattering angles (going down to zero), the uncertainty in the position would be very large, as

can be seen in Fig. 5. As a result of the improved vertex resolution given by the hadrons, the separation of the two target cells becomes possible even for the smallest scattering angles. The probability of an incorrect assignment—for example, the association of the vertex to the wrong target cell—was estimated in bins of  $x$  by a simulation [15]. The resulting reduction of the effective dilution factor, the vertex smearing correction, ranges from about 2% in the highest to 15% in the lowest  $x$  bin.

TABLE III. The asymmetry  $A_1^p(x)$  for the low  $x$  trigger data at the average  $Q^2$  of each  $x$  bin. The first error is statistical and the second is systematic. The first four bins are in the newly accessed kinematic region, while the remaining ones overlap with the standard triggers. The percentage of events overlapping with the standard triggers is given in the last column.

| $x$ range       | $\langle x \rangle$ | $\langle Q^2 \rangle$<br>(GeV <sup>2</sup> ) | $A_1^p$                      | %  |
|-----------------|---------------------|--|------------------------------|----|
| 0.00006–0.00015 | 0.00010             | 0.02   | $0.016 \pm 0.016 \pm 0.008$  | 0  |
| 0.00015–0.00030 | 0.00022             | 0.06   | $0.015 \pm 0.015 \pm 0.005$  | 0  |
| 0.0003–0.0005   | 0.00039             | 0.10   | $0.002 \pm 0.018 \pm 0.002$  | 0  |
| 0.0005–0.0008   | 0.00063             | 0.17   | $-0.004 \pm 0.020 \pm 0.002$ | 0  |
| 0.0008–0.0012   | 0.0010              | 0.26   | $0.021 \pm 0.023 \pm 0.005$  | 12 |
| 0.0012–0.0020   | 0.0016              | 0.40   | $0.045 \pm 0.022 \pm 0.010$  | 21 |
| 0.002–0.003     | 0.0025              | 0.63   | $0.018 \pm 0.026 \pm 0.004$  | 29 |
| 0.003–0.006     | 0.0043              | 1.09   | $-0.007 \pm 0.024 \pm 0.002$ | 35 |
| 0.006–0.010     | 0.0078              | 1.85   | $0.028 \pm 0.030 \pm 0.003$  | 34 |
| 0.010–0.020     | 0.0143              | 3.15   | $0.090 \pm 0.027 \pm 0.006$  | 31 |
| 0.020–0.030     | 0.0245              | 5.10   | $0.073 \pm 0.039 \pm 0.006$  | 32 |
| 0.030–0.040     | 0.0346              | 7.0  | $0.107 \pm 0.052 \pm 0.007$  | 37 |
| 0.040–0.060     | 0.0487              | 9.7  | $0.029 \pm 0.049 \pm 0.003$  | 46 |
| 0.060–0.100     | 0.077               | 14.8   | $0.248 \pm 0.054 \pm 0.016$  | 61 |
| 0.100–0.150     | 0.121               | 23.1   | $0.345 \pm 0.078 \pm 0.020$  | 77 |

TABLE IV. The asymmetry  $A_1^d(x)$  for the low  $x$  trigger data at the average  $Q^2$  of each  $x$  bin, with the same presentation as for Table III.

| $x$ range       | $\langle x \rangle$ | $\langle Q^2 \rangle$<br>(GeV <sup>2</sup> ) | $A_1^d$                      | %  |
|-----------------|---------------------|--|------------------------------|----|
| 0.00006–0.00015 | 0.00010             | 0.02   | $-0.007 \pm 0.034 \pm 0.004$ | 0  |
| 0.00015–0.00030 | 0.00022             | 0.06   | $0.048 \pm 0.033 \pm 0.015$  | 0  |
| 0.0003–0.0005   | 0.00039             | 0.10   | $0.027 \pm 0.039 \pm 0.008$  | 0  |
| 0.005–0.0008    | 0.00063             | 0.17   | $0.043 \pm 0.043 \pm 0.011$  | 0  |
| 0.0008–0.0012   | 0.0010              | 0.26   | $0.030 \pm 0.048 \pm 0.008$  | 15 |
| 0.0012–0.0020   | 0.0016              | 0.40   | $-0.054 \pm 0.045 \pm 0.012$ | 23 |
| 0.002–0.003     | 0.0025              | 0.63   | $-0.012 \pm 0.054 \pm 0.005$ | 31 |
| 0.003–0.006     | 0.0043              | 1.09   | $-0.010 \pm 0.051 \pm 0.005$ | 36 |
| 0.006–0.010     | 0.0078              | 1.85   | $0.039 \pm 0.062 \pm 0.006$  | 34 |
| 0.010–0.020     | 0.0143              | 3.15   | $-0.098 \pm 0.057 \pm 0.008$ | 32 |
| 0.020–0.030     | 0.0245              | 5.09   | $0.010 \pm 0.081 \pm 0.006$  | 32 |
| 0.030–0.040     | 0.0346              | 7.0  | $-0.013 \pm 0.107 \pm 0.006$ | 36 |
| 0.040–0.060     | 0.0487              | 9.6  | $-0.059 \pm 0.102 \pm 0.007$ | 44 |
| 0.060–0.100     | 0.077               | 14.7   | $0.070 \pm 0.113 \pm 0.008$  | 59 |
| 0.100–0.150     | 0.121               | 22.9   | $-0.002 \pm 0.165 \pm 0.006$ | 75 |

Virtual photon asymmetries  $A_1^{p,d}$  for the proton and the deuteron were determined from  $A_{||}^{p,d}$ , according to Eq. (3), and subsequently corrected for the radiative background [13]. Since the presence of a hadron in the final state was required, only contributions from inelastic processes were retained in the calculation, as for the cross sections  $\sigma$  in Eq. (6).

To obtain the asymmetries  $A_1$  information about unpolarized structure functions is required. The dependence of  $A_1$  on  $R = \sigma_L / \sigma_T$  enters through the depolarization factor  $D$  and through the radiative corrections. For  $x > 0.003$  we used the same parametrization of  $R$  as in our previous analysis [4]. For  $x < 0.003$  and  $Q^2 < 1$  GeV<sup>2</sup>, where  $R$  has not been measured, we used the parametrizations of  $\sigma_L$  and  $\sigma_T$  [16] ob-

TABLE V. The spin-dependent structure function  $g_1^p(x)$  for the low  $x$  trigger data at the average  $Q^2$  of each  $x$  bin for  $Q^2 < 1$  GeV<sup>2</sup>. The first error is statistical and the second is systematic, which does not include the uncertainty on  $F_2$ . The value of  $F_2$  taken from the model of Ref. [17] is listed in the last column.

| $\langle x \rangle$ | $\langle Q^2 \rangle$<br>(GeV <sup>2</sup> ) | $g_1^p$                | $F_2^p$ |
|---------------------|--|------------------------|---------|
| 0.00010             | 0.02   | $2.2 \pm 2.2 \pm 0.3$  | 0.028   |
| 0.00022             | 0.06   | $2.0 \pm 2.1 \pm 0.4$  | 0.059   |
| 0.00039             | 0.10   | $0.2 \pm 2.3 \pm 0.2$  | 0.099   |
| 0.00063             | 0.17   | $-0.4 \pm 2.2 \pm 0.2$ | 0.140   |
| 0.0010              | 0.26   | $1.9 \pm 2.1 \pm 0.4$  | 0.184   |
| 0.0016              | 0.40   | $3.2 \pm 1.5 \pm 0.6$  | 0.233   |
| 0.0025              | 0.63   | $0.9 \pm 1.4 \pm 0.2$  | 0.278   |

tained from a fit to the low  $Q^2$  total electron-proton cross section measured at HERA. In the calculation of radiative corrections, in addition to  $R$ , the structure function  $F_2$  down to  $Q^2 = 0$  is also needed. For  $Q^2 > 0.2$  GeV<sup>2</sup> we used the same parametrization of  $F_2$  as in Ref. [4] and below that value the model of Ref. [17].

It was shown in Ref. [4] that the inclusive asymmetry  $A_1$  can be obtained from the sample of events with hadrons if the energy available for the hadronization,  $W$ , is large enough. Indeed, the bias on the asymmetry, because of the loss of inelastic events by the limited acceptance of the spectrometer, was estimated to be smaller than 0.001 for a sample with  $W > 12$  GeV. In the sample analyzed here,  $W$  is comparable and in particular for  $x < 0.002$  it is larger than 15 GeV. For this reason we expect that losses are of the same order as in Ref. [4], i.e., a few percent, and that the bias on the asymmetry  $A_1$  introduced by the hadron requirement can be neglected.

## VI. SYSTEMATIC UNCERTAINTIES IN $A_1$

In our experiment asymmetries are obtained by combining the data taken before and after the reversal of the spin

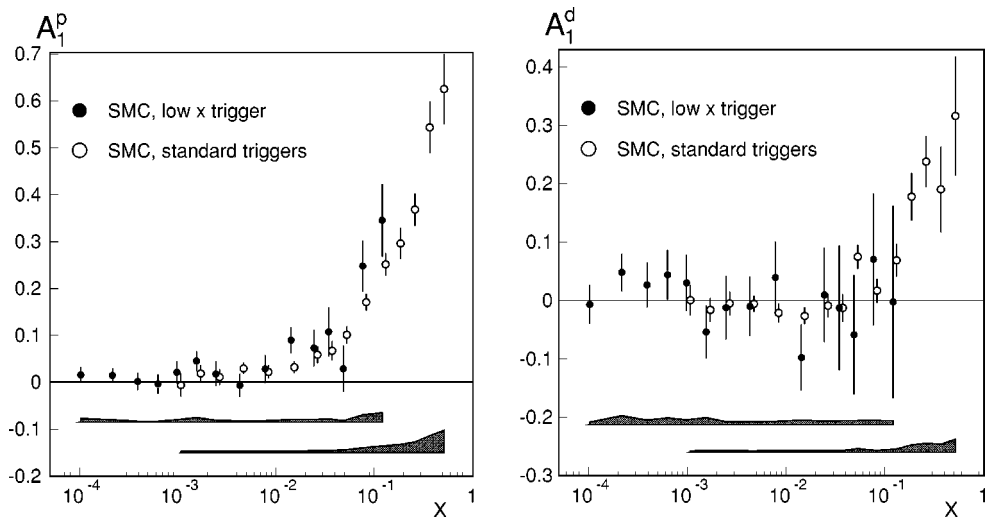


FIG. 6. The asymmetry  $A_1$  for the proton and for the deuteron as a function of  $x$  at the measured  $Q^2$  obtained with the low  $x$  trigger (solid circles) together with those for standard triggers [4] (open circles). The shaded bands indicate the size of the respective systematic errors.

TABLE VI. The spin-dependent structure function  $g_1^d(x)$  for the low  $x$  trigger data at the average  $Q^2$  of each  $x$  bin for  $Q^2 < 1 \text{ GeV}^2$  with the same presentation as for Table V.

| $\langle x \rangle$ | $\langle Q^2 \rangle$<br>(GeV <sup>2</sup> ) | $g_1^d$                | $F_2^d$ |
|---------------------|--|------------------------|---------|
| 0.00010             | 0.02   | $-1.0 \pm 4.7 \pm 0.4$ | 0.028   |
| 0.00022             | 0.06   | $6.4 \pm 4.3 \pm 1.4$  | 0.059   |
| 0.00039             | 0.10   | $3.3 \pm 4.8 \pm 0.9$  | 0.098   |
| 0.00063             | 0.17   | $4.7 \pm 4.6 \pm 1.1$  | 0.140   |
| 0.0010              | 0.26   | $2.7 \pm 4.3 \pm 0.7$  | 0.183   |
| 0.0016              | 0.40   | $-3.8 \pm 3.2 \pm 0.8$ | 0.232   |
| 0.0025              | 0.63   | $-0.6 \pm 2.8 \pm 0.3$ | 0.276   |

orientation in the two target cells [5]. This method leads to a significant reduction of the systematic uncertainties since the muon flux and the spectrometer acceptance need not be known, provided that the ratio of acceptances for events from the two target cells is the same before and after polarization reversal.

A potentially significant contribution to the systematic error is due to false asymmetries generated by instabilities of this acceptance ratio. The time dependence of the efficiencies of different parts of the detector was studied both for the scattered muon and the produced hadrons according to the method described in Ref. [5].

Another possibly important contribution to the systematic error in  $A_1$  for  $x < 0.003$  is due to the uncertainty in the function  $R$ . To estimate this contribution the lower limit  $R = 0$  and the upper limit  $R = 0.5$ , consistent with results of the H1 measurements [18] at low  $x$  and  $Q^2$  about  $10 \text{ GeV}^2$ , were used. For  $x > 0.003$  the uncertainty in  $R$  was calculated as in Ref. [4]. The effects due to uncertainties in  $R$  and  $F_2$  in the computation of the radiative corrections were found to be negligible.

To evaluate the systematic uncertainty in the effective di-

lution factor  $f'$ , we considered contributions from the following sources: the uncertainty in the target composition, the limited precision of the measurements of the structure function ratios  $F_2^A/F_2^d$  [11],  $F_2^d/F_2^p$  [12] and of their extrapolations to the low  $x$  region, the precision of the cross sections in Eq. (6), and the uncertainty in the contamination by  $\mu e$  events and in the vertex smearing correction. As an estimate of the precision of  $\sigma_{1\gamma}^{p,d}/\sigma^{p,d}$  in Eq. (6), we took the difference between results obtained with two calculations [13,14]. Its maximum value is about 5% in the lowest  $x$  bin and below 1% for  $x > 8 \times 10^{-4}$ . The contribution to  $\sigma^{p,d}$  from inelastic scattering with hard photon emission was reduced due to the effective momentum cut in the acceptance for hadrons. A 30% uncertainty was then assigned to this contribution, leading to an additional few percent uncertainty in the ratio  $\sigma_{1\gamma}^{p,d}/\sigma^{p,d}$ .

Other contributions to the systematic uncertainties, non-negligible at higher  $x$ , are the same as in Refs. [4,5]. The individual contributions to the systematic errors in  $A_1^{p,d}$  are presented in Table I for the proton and in Table II for the deuteron.

## VII. RESULTS

The values of the asymmetries  $A_1^{p,d}$  are given in Tables III and IV as functions of  $x$  at the average  $Q^2$  in each bin. The total systematic error in  $A_1$  has been obtained by combining in quadrature the individual contributions described in Sec. VI. In the last column of the tables the percentage of the low  $x$  triggers, simultaneously satisfying at least one of the standard triggers, is given. The overlap increases with increasing  $x$ ; thus, the new data give new information mainly in the low  $x$  and low  $Q^2$  region.

The results on  $A_1^{p,d}$  are presented in Fig. 6. For  $x < 8 \times 10^{-4}$  these are the first measurements of the spin asym-

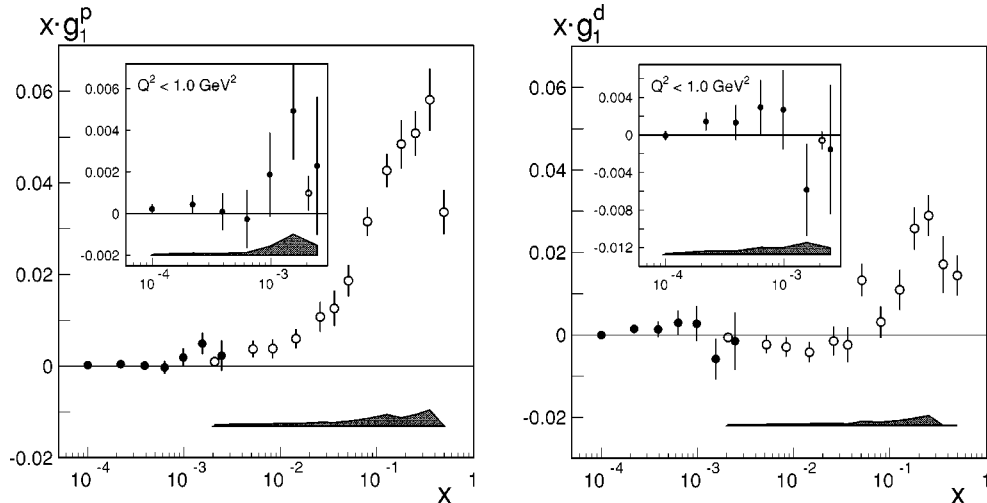


FIG. 7. The values of  $xg_1$  for the proton and for the deuteron as a function of  $x$  at the measured  $Q^2$  obtained with the low  $x$  trigger (solid circles) together with those for standard triggers [4] (open circles). The low  $x$  trigger results are presented in the kinematic region where  $Q^2 < 1 \text{ GeV}^2$ . The shaded bands indicate the size of the respective systematic errors.



metries and are found to be consistent with zero within errors. For larger values of  $x$  the asymmetries from our previous measurements with standard triggers [4] are also shown. In Ref. [4], for  $x < 0.02$ , the presence of a hadron in the final state was required on the off-line level. Taking into account correlations, the two data sets are consistent in the kinematic region of overlap ( $\chi^2/n_{DF} = 12.6/11$  and  $5.5/11$  for the proton and deuteron data, respectively).

The spin structure functions  $g_1$  were calculated only for  $x < 0.003$  and  $Q^2 < 1$  GeV<sup>2</sup> from the results on the asymmetries  $A_1$  using the relation  $g_1 = A_1 F_2 / [2x(1+R)]$ . Here the same values of  $R$  as used in Sec. V have to be taken to be consistent with the  $A_1$  determination; see Eqs. (3),(4). The structure function  $F_2$  was taken from the model of Ref. [17]. The values for  $g_1$  are given in Tables V and VI with the systematic errors resulting from propagation of the error on  $R$  and of the other individual contributions to systematic uncertainties on  $A_1$ . No uncertainty was associated with  $F_2$ . The results for  $xg_1^{p,d}$  are presented in Fig. 7 together with those from Ref. [4]. No significant spin effects are observed in the newly accessed kinematic region.

At small  $x$ , our data cover only very narrow intervals of  $x$  (or  $W$ ) for fixed values of  $Q^2$ ; cf. Fig. 2. Therefore they cannot be compared directly, without additional assumptions about the  $Q^2$  dependence of  $g_1$ , with the Regge model which predicts small  $x$  behavior of  $g_1$  at fixed  $Q^2$ . However, these data can be compared with models predicting both the  $x$  and  $Q^2$  dependence at low values of  $x$  and  $Q^2$ ; see [19].

## VIII. CONCLUSIONS

We have presented measurements of the longitudinal spin asymmetry  $A_1$  for the proton and for the deuteron based on a dedicated low  $x$  trigger involving a hadron requirement. This method strongly reduces the background at low  $x$  and provides the possibility to investigate for the first time the range  $6 \times 10^{-5} < x < 8 \times 10^{-4}$ ,  $0.01 < Q^2 < 0.2$  GeV<sup>2</sup>.

We do not observe any significant spin effects in this kinematic region, while at larger  $x$  the measured asymmetries are in good agreement with our results in Ref. [4].

## ACKNOWLEDGMENTS

We wish to thank our host laboratory CERN for providing major and efficient support for our experiment. We also thank all those people in our home institutions who have contributed to the construction and maintenance of our equipment. This work was supported by Bundesministerium für Bildung, Wissenschaft, Forschung und Technologie, partially supported by TUBITAK and the Center for Turkish-Balkan Physics Research and Application (Bogziçi University), supported by the U.S. Department of Energy, the U.S. National Science Foundation, Monbusho Grant-in-Aid for Science Research (International Scientific Research Program and Specially Promoted Research), the National Science Foundation (NWO) of the Netherlands, the Commissariat à l’Energie Atomique, Comision Interministerial de Ciencia y Tecnologia, the Israel Science Foundation, and Polish State Committee for Scientific Research (KBN) Grant No. 2P03B 081 14 and 2P03B 132 14.

- 
- [1] See, e.g., A. M. Cooper-Sarkar, R. C. E. Devenish, and A. De Roeck, *Int. J. Mod. Phys. A* **13**, 3385 (1998) and references therein.
- [2] ZEUS Collaboration, J. Breitweg *et al.*, *Phys. Lett. B* **407**, 432 (1997); *Eur. Phys. J. C* **7**, 609 (1999); H1 Collaboration, C. Adloff *et al.*, *Nucl. Phys.* **B497**, 3 (1997); see also T. Doyle, plenary talk at the XXIX International Conference on High Energy Physics, Vancouver, Canada, 1998.
- [3] See, e.g., A. Quadt, talk at the XXIX International Conference on High Energy Physics [2].
- [4] SMC, B. Adeva *et al.*, *Phys. Rev. D* **58**, 112001 (1998).
- [5] SMC, D. Adams *et al.*, *Phys. Rev. D* **56**, 5330 (1997).
- [6] SMC, D. Adams *et al.*, *Phys. Lett. B* **336**, 125 (1994); E143, K. Abe *et al.*, *Phys. Rev. D* **58**, 112003 (1998).
- [7] N. Doble *et al.*, *Nucl. Instrum. Methods Phys. Res. A* **343**, 351 (1994).
- [8] SMC, B. Adeva *et al.*, “The polarized double cell target of the SMC,” Report No. CERN-EP/99-31; *Nucl. Instrum. Methods Phys. Res. A* (to be published).
- [9] SMC, B. Adeva *et al.*, *Nucl. Instrum. Methods Phys. Res. A* **343**, 363 (1994); SMC, B. Adeva *et al.*, *Nucl. Instrum. Methods A Phys. Res.* (to be published).
- [10] EMC, O. Allkofer *et al.*, *Nucl. Instrum. Methods* **179**, 445 (1981).
- [11] NMC, P. Amaudruz *et al.*, *Z. Phys. C* **51**, 387 (1991); **53**, 73 (1992); *Nucl. Phys.* **B441**, 3 (1995); M. Arenodo *et al.*, *ibid.* **B441**, 12 (1995); **B481**, 3 (1996).
- [12] NMC, M. Arneodo *et al.*, *Nucl. Phys.* **B487**, 3 (1997).
- [13] T. V. Kukhto and N. M. Shumeiko, *Nucl. Phys.* **B219**, 412 (1983); I. V. Akushevich and N. M. Shumeiko, *J. Phys. G* **20**, 513 (1994).
- [14] A. A. Akhundov *et al.*, *Fortschr. Phys.* **44**, 373 (1996).
- [15] A. Steinmetz, Ph.D. thesis, University of Mainz, 1996.
- [16] B. Surrow, Ph.D. thesis, University of Hamburg, 1998.
- [17] B. Badelek and J. Kwieciński, *Phys. Lett. B* **295**, 263 (1992).
- [18] H1 Collaboration, C. Adloff *et al.*, *Phys. Lett. B* **393**, 452 (1997); M. Klein, talk at the XXIX International Conference on High Energy Physics [2].
- [19] B. Badelek and J. Kwieciński, *J. Phys. G* **25**, 1533 (1999).